$5d$-level energies of Ce^{3+} and the crystalline environment. II. Chloride, bromide, and iodide compounds

P. Dorenbos
Interfaculty Reactor Institute, Delft University of Technology, Mekelweg 15, 2629 JB Delft, The Netherlands
(Received 28 June 2000)

Information on the energy of $5d$ levels of Ce^{3+} in chloride, bromide, and iodide compounds has been collected. From this, values for the centroid shift and the crystal field splitting of the $5d$ configuration are obtained. The centroid shift will be related to the polarizability of the anions and further analyzed by means of the ligand polarization model. The crystal field splitting is to a large extent determined by the shape and size of the anion polyhedron coordinating Ce^{3+}. It will be analyzed in terms of the crystal field B_q^k parameters. By combining centroid shift and crystal field splitting, the spectroscopic redshift of the first electric dipole-allowed fd transition in Ce^{3+}-doped halide compounds will be interpreted. The observed trends provide insights into the relationship between the spectroscopic properties of Ce^{3+} $5d$ levels and the crystalline environment.

I. INTRODUCTION

The first allowed $4f^n \rightarrow 4f^{n-1}5d$ transition of the free trivalent lanthanides is lowered in energy whenever it is put in a crystalline environment. This lowering is known as the spectroscopic redshift and in Ref. 1 and Ref. 2 it was shown that for all the trivalent lanthanides it is about the same if put in the same host crystal. It implies that once the first allowed fd transition is known for just one of the trivalent lanthanides, then that of all others if in the same crystal can be predicted. This knowledge provides a powerful predictive tool. However, one likes to go beyond this and also understand the relationship between redshift and the type of crystalline environment of the lanthanide ion. One may then hope to predict the redshift in yet uninvestigated new compounds.

This paper is Part II in a series of papers where this relationship is the subject of study. In the first paper,[3] hereafter referred to as Part I, the fluorides were treated. In this second part, the other halides (chlorides, bromides, and iodides) are the subject of study. The physical (like ionic radius) and chemical (like reducing character) properties of the halides in going from F^- to Cl^- to Br^- to I^- change considerably. It has profound consequences for the position of the $5d$ levels of lanthanide doped halide compounds.

The redshift or depression value $D(A)$ in compound A is related to the centroid shift $\epsilon_c(A)$ of the $5d$ configuration and the total crystal field splitting ϵ_{cfs} via

$$D(A) = \epsilon_c(A) + \frac{\epsilon_{cfs}(A)}{r(A)} - 1890 \ \text{cm}^{-1}, \tag{1}$$

where $1/r(A)$ is the fraction of the crystal field splitting that adds to the redshift. To understand the relationship between the redshift and the type of crystalline environment one needs information on all $4f^{n-1}5d$-level energies. This is only feasible for Ce^{3+}. It has the simplest spectroscopy, and, depending on the site symmetry, at most five energetically different $5d$ levels can be observed. New data and information gathered from literature provided the required information on 16 different compounds.

The model of ligand polarization formulated in Part I will be used to interpret the values for the centroid shift. It relates $\epsilon_c(\text{cm}^{-1})$ to the N coordinating anion ligands at distance R_i (pm) from Ce^{3+} via

$$\frac{\epsilon_c}{N} = \frac{1.44 \times 10^{17} \alpha_{sp}}{R_{eff}^6}, \tag{2}$$

where R_{eff} is defined as

$$\frac{1}{R_{eff}^6} \equiv \frac{1}{N} \sum_{i=1}^{N} \frac{1}{(R_i - \frac{1}{2}\Delta R)^6}. \tag{3}$$

α_{sp} in units of 10^{-30} m^3 or Å^3 is a parameter that is related to the polarizability of the halide ions. Since its value is calculated from spectroscopic information on $5d$ levels, it is called the spectroscopic polarizability. ΔR is the difference in ionic radius of Ce^{3+} with the ion it substitutes for. To account roughly for lattice relaxation it was assumed that the neighboring anions relax outward or inward by just half this difference. For the fluorides it was found (Part I) that the magnitude of α_{sp} compares well with experimentally determined polarizabilities (α_{exp}) of fluoride ions in ionic crystals. It varies in a systematic way with the radii and valency of the cations present in the lattice. Small highly charged cations appear to reduce α_{sp}. Large monovalent or divalent cations have the opposite effect. In this second part these systematics will be further established.

In this series of papers where among other properties, the crystal field splitting in a wide variety of materials is studied, a phenomenological approach will be taken for its interpretation. There appears a clear relationship between the type (shape) of anion coordination polyhedron around Ce^{3+} and ϵ_{cfs}. The point charge electrostatic model (PCEM) of crystal field interaction will be used to further analyze this relationship. Although the model will prove very helpful to understand the influence of polyhedral shape, it cannot be used for quantitative predictions. By comparing ϵ_{cfs} in compounds

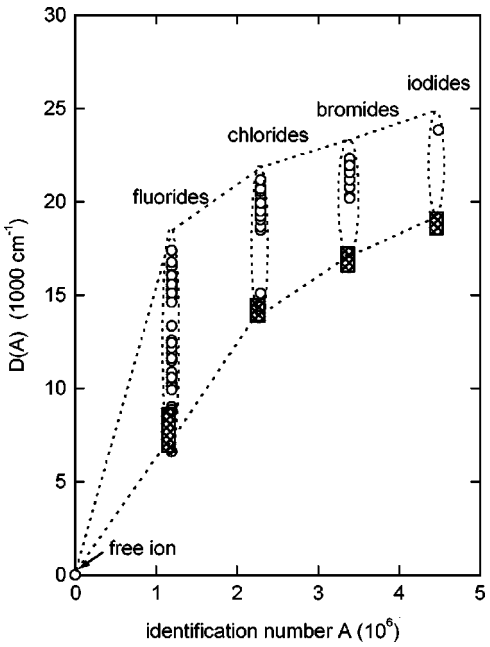

FIG. 1. Spectroscopic redshift of the trivalent lanthanides in the halogenide compounds (from Ref. 2). The hatched blocks represent the observed or predicted range of centroid shift values ϵ_c.

with similar coordination polyhedra but of different size, empirical relationships between ϵ_{cfs} and Ce^{3+}-anion distance will be established.

II. EXPERIMENTAL DATA ON 5d-LEVEL POSITIONS

The available data on the spectroscopic redshift $D(A)$ of the halide compounds as tabulated in Ref. 2 can be seen in Fig. 1. The data are shown against a seven-digit identification number. Such number was assigned to each of the compounds and when treated as a running variable (A) it enables one to present and analyze the data in a systematic manner. The reader is referred to Ref. 2 for more information and motivation of the chosen classification scheme. On the scale in Fig. 1, the first two digits, which represent the types of anions in the host crystal, are of significance. A first inspection shows that the redshift tends to increase in going through the halide series from the fluorides to the iodides. The spread in redshift values is largest within the fluorides and tends to decrease in going to chlorides and bromides.

Of several Ce^{3+} activated compounds, information is available on the energy of all five 5d levels. The wavelengths of fd transitions are compiled in Table I (see column 4). In cases when the fd transition wavelengths are not yet fully certain like in Cs_2LiYBr_6, they are placed between brackets. In the case of octahedral or near octahedral (trigonal antiprism) symmetry, some of the fd transition were assumed to be to twofold or threefold degenerate 5d levels. This is indicated by $(2\times)$ or $(3\times)$. From the wavelengths the centroid shift and crystal field splitting were calculated.

The second and third columns give information on the size and type of anion polyhedron coordinating Ce^{3+}. The size is expressed as the average distance R_{av} to the N coordinating anions: it was determined from crystallographic data. Occasionally R_{av} was estimated by comparison with isostructural compounds and correcting for differences in cell volume or cation ionic radii.

The energy of the highest 5d level, the centroid position, the energy of the lowest 5d level, and the energy of emission from the relaxed lowest 5d level to the $^2F_{5/2}$ ground state are shown in Fig. 2. All energies are relative to the centroid position of the free Ce^{3+} ion located at 51 230 cm^{-1}. The differences between the relaxed and unrelaxed lowest

TABLE I. Spectroscopic and crystallographic properties of Ce^{3+}-doped chloride and bromide compounds. R_{av} is in pm. Type of polyhedron (poly) and point symmetry (sym) at the Ce site are given.

compound	(N:R_{av})	(poly:sym)	5d-excitation bands (nm)	ϵ_c(cm^{-1})	ϵ_{cfs}(cm^{-1})	Ref.
$LaCl_3$	(9:295)	(3ctp:C_{3h})	243, 250, 263, 274, 281	13000	5565	13
$CaCl_2$	(6:275)	(tap:C_{2h})	242, 252, 266, 277, 292	13440	7075	4
cubic-$BaCl_2$	(8:329)	(cubal:O_h)	235, 245, 255, 316, 325	14390	12610	4
$SrCl_2$:(C_{4v})	(9:307)	(1ccubal:C_{4v})	(224),233,240,(255), $(2\times)$324	≈13580	≈12900	4
K_2LaCl_5	(7:≈285)	(1ctp:C_s)	221, 239, 258, 316, 337	13710	15128	26
$CsSrCl_3$	(6:≈280) [a]	(tap:≈O_h)	219, . . . , 332		15542	6
$KCaCl_3$	(6:≈261) [a]	(tap:≈O_h)	210, . . . , 338		18033	6
$RbCaCl_3$	(6:≈266) [a]	(tap:≈O_h)	214, 220, $(3\times)$342	15250	17489	6
$Cs_2NaLaCl_6$	(6:≈275) [b]	(octa:O_h)	210, 217, 336, $(2\times)$342	14742	18379	28
$Cs_2NaGdCl_6$	(6:≈265) [b]	(octa:O_h)	(211, 216), (330), $(2\times)$350	≈15003	≈18822	29
Cs_2NaYCl_6	(6:262)	(octa:O_h)	(210, 217), 331, $(2\times)$345	≈14854	≈18634	29,30
$Cs_2NaLuCl_6$	(6:≈259) [b]	(octa:O_h)	205, 215, 337, $(2\times)$355	14969	20611	28
Cs_2LiYCl_6	(6:263)	(octa:O_h)	207, 217, 327, $(2\times)$349	14774	19656	29,31
$LuCl_3$	(6:≈258) [c]	(tap:C_2)	196, 217, 325, $(2\times)$340	13891	21609	33
Cs_2LiYBr_6	(6:≈277) [b]	(tap:C_2)	$(2\times)$235,(340),$(2\times)$(360)	≈17215	≈14775	29
$LuBr_3$	(6:≈274) [d]	(tap:C_2)	$(2\times)$229, 342, 356, 370	16892	16641	33

[a]See Ref 27.
[b]R_{av} was estimated from the lattice parameters from Ref. 7 and the ratio of cationic radii from Ref. 18.
[c]See Ref 32.
[d]See Ref 34.

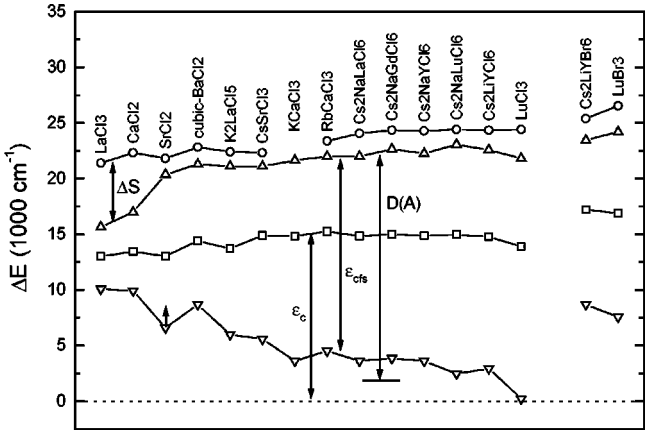

FIG. 2. Energy differences between the centroid position (51 230 cm^{-1}) of the free Ce^{3+} ion and (∇) highest $5d$ level, ($\square$) centroid position, ($\triangle$) lowest $5d$ level, and ($\bigcirc$) relaxed lowest $5d$ level of Ce^{3+} in compounds.

$5d$-level energy is the Stokes shift ΔS: their values can be found in Ref. 2. The chloride compounds in Fig. 2 and Table I are more or less arranged in order of increasing size of the crystal field splitting and decreasing coordination number around Ce^{3+}.

III. DISCUSSION

The crystal structure of the different compounds, particularly the type of anion polyhedron coordinating Ce^{3+}, and how it influences the crystal field splitting will be discussed first. From this, several trends will emerge. Next, the relationship between ϵ_{cfs} and polyhedral shape will be further analyzed employing the point charge electrostatic model. It will be followed by a discussion on the centroid shift analyzed employing the ligand polarization model. Finally the ideas are combined to interpret the redshift of all halide compounds. It appears that the centroid shift in chlorides and bromides is several times larger than that in fluorides, but the crystal field splitting appears much smaller. The former is attributed to increasingly larger anion polarizability and covalency effects in going through the halide series. By means of the parameter α_{sp} these two effects are more or less quantified. The latter is attributed to the increase of anion size yielding larger distances between Ce^{3+} and the anion ligands.

A. Crystal field splitting

Figure 3 shows ϵ_{cfs} plotted against $R_{av}-\frac{1}{2}\Delta R$ for most of the compounds from Table I. Also data on the fluorides from Part I have been used. Like in Eq. (3), $\frac{1}{2}\Delta R$ accounts roughly for the lattice relaxation around Ce^{3+}. The straight dashed lines more or less connect the data of compounds with similar type of coordination polyhedron. From top to bottom these are the trigonal antiprism (tap), cube (cubal), dodecahedron (ddh), tricapped trigonal prism (3ctp), and cuboctahedron (6ctap). The straight solid lines with steeper slope more or less connect data of compounds with similar coordination polyhedron and with similar anions (F, Cl, or Br).

$LaCl_3$ shows the smallest crystal field splitting of all compounds. The La^{3+} site is ninefold coordinated by chlorine in

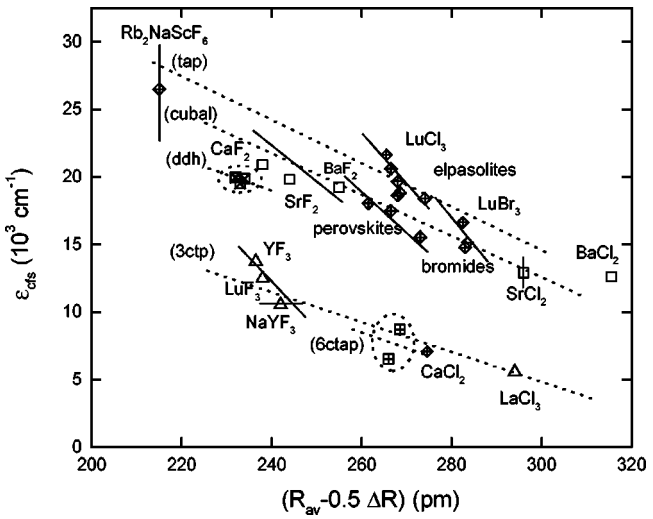

FIG. 3. Crystal field splitting ϵ_{cfs} of Ce^{3+} in halides. Different data symbols were chosen to distinguish compounds with different types of anion coordination polyhedron.

the form of a regular tricapped trigonal prism (3ctp:C_{3h}). Compared to $NaYF_4$, see Part I, with similar coordination but smaller $R_{av}-\frac{1}{2}\Delta R$, the splitting is almost two times less.

Cubic-$BaCl_2$ (8:329) and $SrCl_2$ (8:302) have the cubic fluorite crystal structure. The Ce ion is in a site with cubal eightfold coordination. In $SrCl_2$ the excess charge is compensated by means of a Cl^- ion at the nearest interstitial site (349 pm) resulting in a monocapped cubal polyhedron (1ccubal) with C_{4v} site symmetry. No information is available on the type of charge compensating defect in $BaCl_2$. The excitation spectra of Ce^{3+} luminescence reported by Li and Leskelä[4] can be interpreted as two low-energy levels arising from the doublet e state plus three high-energy levels from the triplet t states. It is not clear whether the 224-nm or the 255-nm band, see Table I, in $SrCl_2$:Ce belongs to this triplet. Possibly the 255-nm band is like other bands between 260 and 300 nm caused by aggregates of Ce^{3+} ions, see Refs. 4 and 5. Crystal field splitting of the cubic chlorides together with those of the cubic fluorites CaF_2,SrF_2, and BaF_2 are shown in Fig. 3. For these data, $R_{av}-\frac{1}{2}\Delta R$ represents the eight cubal halide ions, and the charge compensating anion was not included. Crystal field splitting in the chlorides is significantly smaller than in the fluorides.

In most of the compounds of Table I Ce^{3+} is coordinated in the form of a (distorted) octahedron. In the chloride elpasolite $Cs_2NaLaCl_6$, ϵ_{cfs} is 18 400 cm^{-1} and it increases with decreasing size of the rare-earth cation until 20 600 cm^{-1} for $Cs_2NaLuCl_6$, see also Fig. 2. The largest crystal field splitting amongst the chlorides is observed for $LuCl_3$. The data on crystal field splitting in $LuBr_3$ and Cs_2LiYBr_6 can also be found in Fig. 3. It is about 5000 cm^{-1} smaller than in the corresponding $LuCl_3$ and Cs_2LiYCl_6 compounds.

In Fig. 3, the octahedral (trigonal antiprism) crystal field splitting of the different compounds, including that of Rb_2NaScF_6 (see Part I), is shown. Octahedral splitting seems somewhat larger than that of cubal coordination. Compared to compounds with tricapped trigonal prism or cuboctahedral coordination, crystal field splitting appears about two times larger.

From fluorides to chlorides to bromides the ionic radius of the halide ion increases from 133 pm to 181 pm to 196 pm resulting in larger R_{av}. The dashed lines in Fig. 3 demonstrate that the rate of decrease of ϵ_{cfs} with increase of halide ion size seems about the same for (tap), (cubal), and (3ctp) type of coordination.

The above characteristics can be exploited to interpret the excitation spectra of Ce^{3+} luminescence in three distorted perovskite-type chloride crystals reported by Antonyak *et al.*[6] The excitation spectra of $CsSrCl_3$ and $KCaCl_3$ show more than five bands indicating that different Ce^{3+} sites are present. It may be related with the manner of charge compensation. Antonyak *et al.* assume Ce^{3+} to occupy the 12-fold coordinated monovalent cation site. However, based on the data in Fig. 3, the crystal field splitting of these large cuboctahedral sites is expected to be less than 8000 cm^{-1}. The actual splitting is two times larger, which suggests that the distorted octahedral divalent cation site is occupied by Ce^{3+}. The excitation spectrum of $RbCaCl_3$ shows three bands. Assuming approximately octahedral coordination, the 342-nm excitation is assigned to the triplet t_2 5d level and the bands at 214 and 220 nm to the split doublet e 5d level. All wavelengths are shown in Table I.

K_2LaCl_5 is isotypic with K_2PrCl_5 and has sevenfold coordination[7] in the form of a monocapped trigonal prism (1ctp). Crystal field splitting of K_2LaCl_5 is quite comparable with that of octahedral coordination.

The last chloride compound to be discussed is $CaCl_2$, which shows an unexpectedly small crystal field splitting of 7100 cm^{-1}. A value of around 17 000 cm^{-1} for the sixfold coordinated Ca site in the rutile structure of $CaCl_2$ seems to be a more likely value, see Fig. 3. Possibly coordination is different from octahedral due to lattice relaxation or charge compensating defects. This will be discussed in more detail later.

B. Angular part of the B_0^2 and B_0^4 crystal field parameters

The results in Fig. 3 show that the crystal field splitting depends on the type of anion polyhedron around Ce^{3+}. This dependence will be further analyzed by employing the PCEM of crystal field interaction. The interaction is simplified by assuming that only the nearest-neighbor anions, forming a polyhedron around Ce^{3+}, contribute to the crystal field potential at the Ce^{3+} site. It is further assumed that all Ce to anion distances (R_i) are equal. In this work, the model will be applied to crystals with anion coordination polyhedra that can be seen as a combination of 2m prismatic, n equatorial and p axial ligands. The prismatic ligands form a prism or anti-prism with its m-fold rotation axis defined as the z axis of our coordinate system. The equatorial or planar ligands are located in the x-y plane forming caps on the side faces of the (anti)prism. The y axis is coincident with a twofold symmetry axis of the polyhedron. The axial ligands located on the z axis form caps on the top and/or bottom faces of the (anti)prism.

For these polyhedral types, generalized expressions can be obtained for the so-called B_q^k crystal field parameters.[8] In the case of 5d levels, the integer k is restricted to 0, 2, and 4 and integer q is a multiple of m and $\leqslant k$. Of special interest are the B_0^2 and B_0^4 parameters. It is well known that the PCEM is too naive a model for a reliable calculation of crystal field parameters. Nevertheless, it will prove useful to relate qualitatively polyhedral shape with crystal field splitting. For that purpose only the so-called angular part of the crystal field parameters will be used. They will be denoted as Θ_q^k and can be written as a sum of an axial, equatorial, and prismatic contribution. The ones of interest are[8]

$$\Theta_0^2 = p - \frac{n}{2} + m(3\cos^2\theta_{pr} - 1), \tag{4}$$

$$\Theta_0^4 = p + \frac{3n}{8} + \frac{m}{4}(35\cos^4\theta_{pr} - 30\cos^2\theta_{pr} + 3). \tag{5}$$

The prismatic angle θ_{pr} is the angle the 2m ''prismatic'' Ce^{3+}-halide bonds make with the m-fold axis. The expressions are the same for prismatic and antiprismatic coordination. The values for Θ_q^k reflect how the spatial arrangement of the anions, i.e., the shape of the polyhedron, influence the crystal field parameters.

Most of the coordination polyhedra in the compounds treated in this work can be seen as containing a trigonal (anti)prismatic part with (approximately) threefold rotation symmetry. The crystal field parameters of the cube, octahedron, and cuboctahedron are usually described with the fourfold symmetry axis as quantization axis. However also a threefold rotation symmetry axis can be chosen. The cube is then seen as a (2ctap) biaxially capped trigonal antiprism (p:n:m)=(2:0:3), the octahedron as trigonal antiprism (tap), and the cuboctahedron as a sixequatorially capped trigonal antiprism (6ctap). This latter view is preferred here because it provides a direct comparison with many of the polyhedra lacking fourfold rotation symmetry.

In Table II information on several types of polyhedra with threefold symmetry axis ($m=3$) is compiled. Typical values for the prismatic angle θ_{pr} can be obtained from real crystallographic structures or calculated using, for example, the hard sphere model (HSM).[8,9] The HSM value for the trigonal prism is 49°. Adding three equatorial ligands on the square faces to form the tricapped trigonal prism elongates the prism and $\theta_{pr}=\arcsin(2/3)=41.8°$.[9] This HSM value is indeed observed in the $LaCl_3$ structure. θ_{pr} is slightly smaller ($\approx 41°$) in $NaYF_4$. Adding three more equatorial caps results in the anticuboctahedron (6ctp) with $\theta_{pr}=35.3°$, a coordination type found in several hexa-aluminates like $SrAl_{12}O_{19}$. Axial ligands have an opposite effect, i.e., the prism is flattened and θ_{pr} increases. In LaF_3 with the thysonite structure, two axial and three equatorial ligands are present forming a five-capped trigonal prism (5ctp). The polyhedron is quite distorted and three θ_{pr} values of 60°,62°, and 66° are obtained from the structure reported by Zalkin and Templeton.[10]

The octahedron is a trigonal antiprism with θ_{pr} equal to the so-called cubic angle $\theta_c=\arccos(1/\sqrt{3})=54.7°$. The effects of axial and equatorial ligands on the prismatic angle are quite similar as on the trigonal prism. Six equatorial ligands to form a cuboctahedron reduces θ_{pr} to 35.3° (i.e., $90°-\theta_c$). Two axial ligands yield the cube with larger $\theta_{pr}=70.5°$ (i.e., $180°-2\theta_c$).

TABLE II. Angular part Θ_q^k of the B_0^2 and B_0^4 crystal field parameters calculated with the point charge electrostatic model for regular coordination polyhedra with a threefold rotation axis ($m=3$).

(poly:sym)	$(p:n:\theta_{pr})$	Example	Θ_0^2	Θ_0^4
(2ctap:O_h)	(2:0:70.5°)	fluorites	0	2.07
(5ctp:D_{3h})	(2:3:60°)	thysonites	−0.25	1.39
(tap:O_h)	(0:0:54.7°)	elpasolites	0	−2.33
(tp:D_{3h})	(0:0:49°)	HSM-value	0.87	−2.57
(1ctp:C_{2v})	(0:1:≈47°)	K_2PrCl_5	0.69	−2.16
(3ctp:D_{3h})	(0:3:42°)	$LaCl_3$	0.34	−1.15
(6ctp:D_{3h})	(0:6:35.3°)	hexa-aluminates	0	1.17
(6ctap:O_h)	(0:6:35.3°)	perovskites	0	1.17

The different contributions to the angular part of B_0^2 are shown in Fig. 4. The solid line represents the contribution from the prismatic ligands. Despite a strong variation in this contribution with θ_{pr}, the total angular part of B_0^2 remains close to zero for the polyhedra of Table II. The six equatorial caps in the cuboctahedron and the two axial ones in the cube fully cancel the prismatic contribution resulting in zero value for B_0^2. A similar cancellation is observed for the tricapped and five-capped trigonal prism also resulting in relatively small value for the angular part of B_0^2 (see Table II).

Figure 5 shows the contributions to the angular part of the B_0^4 parameter. The prismatic contribution is large and negative for the trigonal prism and the octahedron. It is close to zero for the cube. Equatorial and axial ligands have positive contributions and may compensate (tricapped trigonal prism) or overcompensate (cuboctahedron) for the prismatic contribution. In the case of octahedral, cubal, and cuboctahedral coordination, one obtains the familiar result[8,11] that $\Theta_0^4(\text{cubal}) = -\frac{8}{9}\Theta_0^4(\text{octa})$ and $\Theta_0^4(\text{cubo}) = -\frac{1}{2}\Theta_0^4(\text{octa})$. For (3ctp) and (5ctp) coordination the PCEM predicts $\Theta_0^4(3\text{ctp}) \approx \frac{1}{2}\Theta_0^4(\text{octa})$ and $\Theta_0^4(5\text{ctp}) \approx -0.6\Theta_0^4(\text{octa})$.

Comparing the absolute values for the angular part of the B_0^4 parameter, see Table II, with observed crystal field splitting in Fig. 3 one observes similar ratios. Indeed experimentally, if $R_{\text{av}} - \frac{1}{2}\Delta R$ remains constant, octahedral and cubal crystal field splitting are about the same and two times larger than cuboctahedral and (3ctp) crystal field splitting. Also the crystal field splitting of K_2LaCl_5 with (1ctp) coordination follows the size of the angular part of the B_0^4 parameter. It seems that for polyhedral types as in Table II this parameter is very important for the crystal field splitting; the B_0^2 parameter seems to be of less importance. It is noted that polyhedra containing a trigonal antiprism also have a nonzero B_3^4 parameter. It will mix different $5d$ states but it is not believed to effect ϵ_{cfs} to a large extent, see also Sec. 2.7.2 in Ref. 8. For polyhedral coordination types as in Table II, it is now concluded that the magnitude of the angular part of the B_0^4 parameter as calculated from the PCEM is proportional to the total crystal field splitting.

Equation (4) and Eq. (5) can also be used to predict the effects of polyhedral distortions and charge compensating defects on crystal field splitting. If the fourfold rotation axis is chosen as quantization axis, the angular part of B_0^4 equals −3.11 for cubal coordination with $(p:n:m:\theta_{pr}) = (0:0:4:54.7°)$. The interstitial charge compensating halide ion in SrF_2, CaF_2, and $SrCl_2$ can now be seen as an axial ligand at $2/\sqrt{3} = 1.15$ times larger distance than the prismatic ones. It will reduce the magnitude of the angular part of the

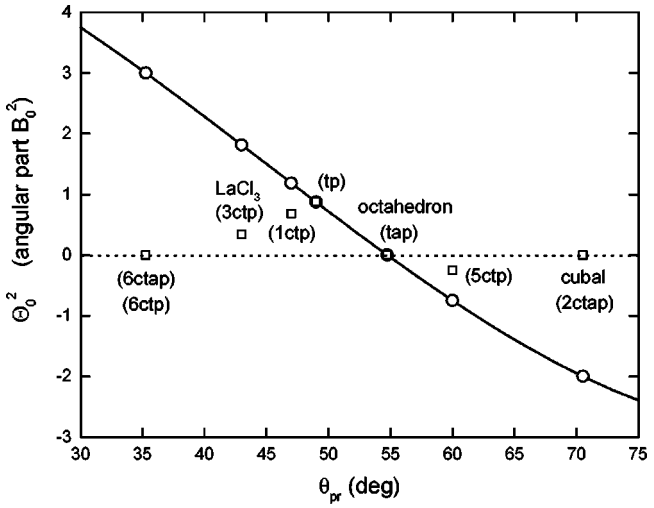

FIG. 4. The angular part Θ_0^2 of the B_0^2 crystal field parameter for several polyhedra with the threefold rotation axis defined as z axis. Solid curve, contribution from the prismatic anions. □, all contributions included.

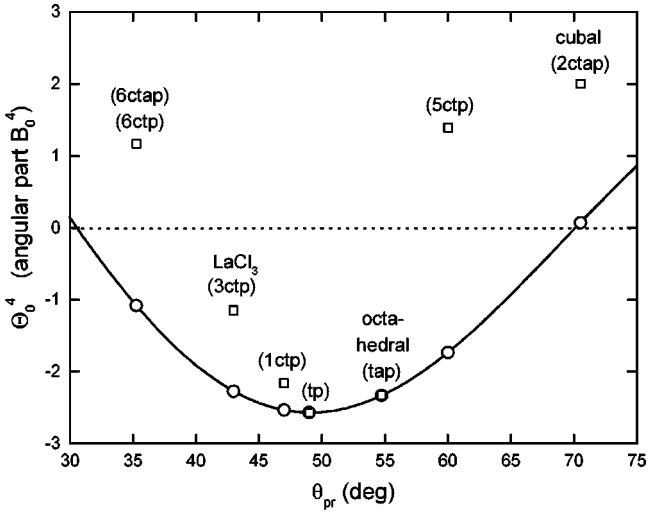

FIG. 5. The angular part Θ_0^4 of the B_0^4 crystal field parameter for several polyhedra with the threefold rotation axis defined as z axis. Solid curve, contribution from the prismatic anions. □, all contributions included.

B_0^4 parameter, see Eq. (5). Treating again Θ_0^4 as an indicator for crystal field strength, it implies that the actual cubal crystal field splitting in CaF_2, SrF_2, and $SrCl_2$ is larger than that suggested by the data in Fig. 3. The difference may amount to several thousand cm^{-1}.

Polyhedral distortion may also explain the large Stokes shift that is observed whenever the coordination is cuboctahedral, tricapped trigonal prism, or five-capped trigonal prismlike, see also Part I and Ref. 12. With Ce^{3+} in the ground state, the polyhedron is regular yielding small crystal field splitting. Upon excitation to the 5d configuration, the lattice will relax. Since crystal field splitting was already minimal, any distortion of the polyhedron will result in an enhancement of crystal field splitting. Effectively the lowest 5d level is further lowered in energy resulting in a large Stokes shift. Recent *ab initio* studies performed by Andriessen *et al.*[13] on $LaCl_3:Ce^{3+}$ and by Marsman *et al.*[14] on $BaLiF_3:Ce^{3+}$ indeed revealed these mechanisms.

Figure 3 shows data belonging to $LiYF_4$, $LiLuF_4$, BaY_2F_8, and $BaLu_2F_8$, each with dodecahedral type of coordination. All data fall close together and crystal field splitting is at least several thousand cm^{-1} smaller than what one would expect in the case of cubal coordination. A dodecahedron does not possess an axis of threefold symmetry and its crystal field parameters therefore cannot be compared directly with those in Table II. Comparison with a cube is possible by treating the cube as two (interpenetrating) regular tetrahedra, i.e., two $m=2$ antiprisms with twofold symmetry axis and $\theta_{pr}=\theta_c=54.7°$.[8] In the scheelite $LiYF_4$ (see Part I), one tetrahedron is elongated ($\theta_{pr}=\theta_c-17°$) and the other is squat ($\theta_{pr}=\theta_c+12°$). It yields a polyhedron with 12 triangular faces (dodecadeltahedron).

The 5d-excitation spectrum of Ce^{3+} in $LiYF_4$ was recently analyzed in terms of the B_q^k crystal field parameters by Reid *et al.*[15] Approximating the actual S_4 symmetry by D_{2d}, values of 10 519 cm^{-1} and $-24\,549$ cm^{-1} were reported for B_0^2 and B_0^4, respectively. Employing Eq. (4) and Eq. (5), values of $+0.64$ and -1.45 are calculated for Θ_0^2 and Θ_0^4. Note that the proper signs for the crystal field parameters are predicted by the PCEM. Properties of $LiYF_4$ can best be compard with those of CaF_2 with only few pm larger R_{av}. A value of $-36\,600$ cm^{-1} was reported by Manthey[16] for the B_0^4 parameter of the Ce^{3+} C_{4v} center in CaF_2. This much larger value as compared to that of $LiYF_4$ is also predicted from the PCEM where a value of -3.11 is obtained for Θ_0^4.

C. Centroid shift

The average centroid shift in the chloride compounds amounts to 13 500 cm^{-1}, which is more than two times larger than the average observed for fluoride compounds (see Part I). This large centroid shift and the slight but significant variations therein can be studied in more detail employing the ligand polarization model as expressed by Eq. (2).

In Fig. 6 the average centroid shift contribution by each of the coordinating anions is plotted against the effective distance defined in Eq. (3). Some curves demonstrating the $R_{\rm eff}^{-6}$ dependence are also shown. In Fig. 7 the same data together with those of the fluorides presented in Part I are shown.

The results reveal that despite the large effective metal to ligand distances in the chlorides, the contribution to the centroid shift per Cl^- is several times larger than the contribution per F^- ion. This is also reflected in the value for the parameter $\alpha_{\rm sp}$ calculated from the observed centroid shift and compiled in Table III. For chlorides it appears to be about 6–8 times larger than for the corresponding fluoride compounds. Compared to this large increase, the further increase in going to the bromides is relatively modest. Within the chlorides one observes that the smallest values for $\alpha_{\rm sp}$ are obtained when small cations like Lu^{3+} are present in the structure. Presence of large cations like Ba^{2+} or Sr^{2+} yield large values for $\alpha_{\rm sp}$. The same was observed for the fluorides in Part I. There it was explained by the attracting force on the anion charge cloud towards the cations. If it is large, as when small Lu^{3+} ions are present, the anion electrons are more strongly bound resulting in larger oscillation force constants and smaller polarizability. The value for cubic-$BaCl_2$ ($\alpha_{\rm sp}=12.3$ Å^3) seems somewhat large. If one assumes the presence of a charge compensating chlorine ion at the nearest interstitial site a somewhat smaller value of

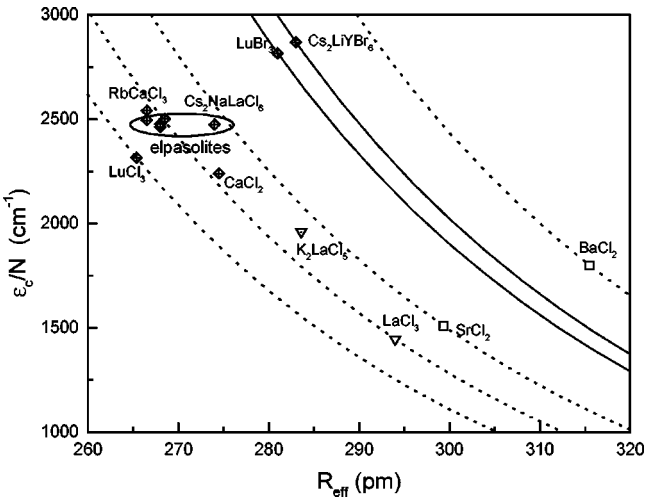

FIG. 6. The centroid shift ϵ_c per coordinating halide ion (N). The curves through some of the data show the dependence on $R_{\rm eff}$.

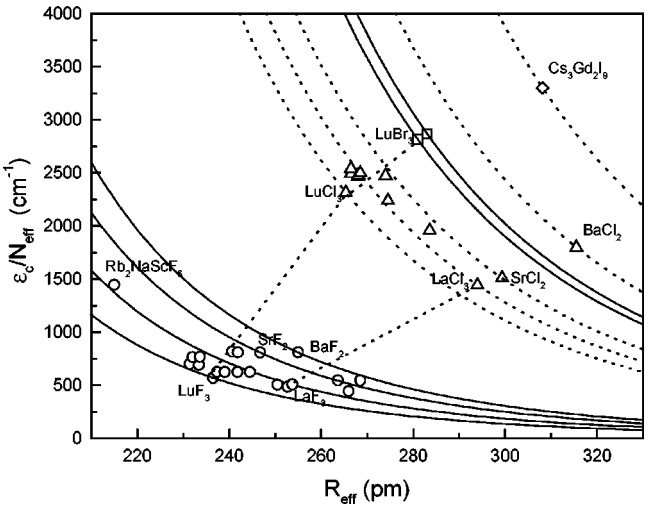

FIG. 7. The centroid shift per coordinating halide ion. ○, the fluorides; △, the chlorides; □, the bromides; ◇, predicted value for $Cs_3Gd_2I_9$. The curves throught the data show the dependence on $R_{\rm eff}$.

TABLE III. Results from the ligand polarization model. Compounds are arranged according to increase of α_{sp}. The entries for $Cs_3Gd_2I_9$ are predicted values.

Compound	R_{eff} (pm)	$\epsilon_c/N(cm^{-1})$	$\alpha_{sp}(10^{-30}\ m^3)$
chlorides			
$LuCl_3$	265	2315	5.61
$Cs_2NaLuCl_6$	267	2495	6.21
$RbCaCl_3$	267	2542	6.32
Cs_2LiYCl_6	268	2462	6.34
Cs_2NaYCl_6	268	2476	6.37
$LaCl_3$	294	1444	6.48
$Cs_2NaGdCl_6$	269	2501	6.51
$CaCl_2$	275	2240	6.65
K_2LaCl_5	284	1959	7.08
$Cs_2NaLaCl_6$	274	2474	7.27
$SrCl_2$	299	1509	7.5 ± 0.5
cubic-$BaCl_2$	319	1800	12.3
bromides			
$LuBr_3$	281	2815	9.62
Cs_2LiYBr_6	283	2869	10.2
iodides			
$Cs_3Gd_2I_9$	(308)	(3300)	(19.6 ± 1.1)

11.7 Å^3 would be obtained. The error can also be quite large because of the large value for $\Delta R=27$ pm for Ce^{3+} on a Ba^{2+} site.

A further test of the ligand polarization model is by comparing the value for the spectroscopic polarizability α_{sp} with actual in-crystal halide polarizabilities derived from macroscopic parameters like the refractive index or dielectric constant of the host crystals. Figure 8 shows the anion polarizability in the alkali halides and some alkaline-earth halides obtained from the work by Pearson *et al.*[17] α_{exp} is shown against the ionic radius of the cations obtained from Shannon.[18] α_{exp} and α_{sp} behave quite similarly. Within the fluorides and within the chlorides both increase with increasing size of the cations present in the structure. A large increase of α_{exp} is observed in going from fluorides to chlorides. The increase from chlorides to bromides is less pronounced. Similar features are observed for α_{sp}, cf. the data for LuF_3 ($\alpha_{sp}=0.69$ Å^3), $LuCl_3$ ($\alpha_{sp}=5.6$ Å^3), and $LuBr_3$ ($\alpha_{sp}=9.6$ Å^3) in Fig. 7.

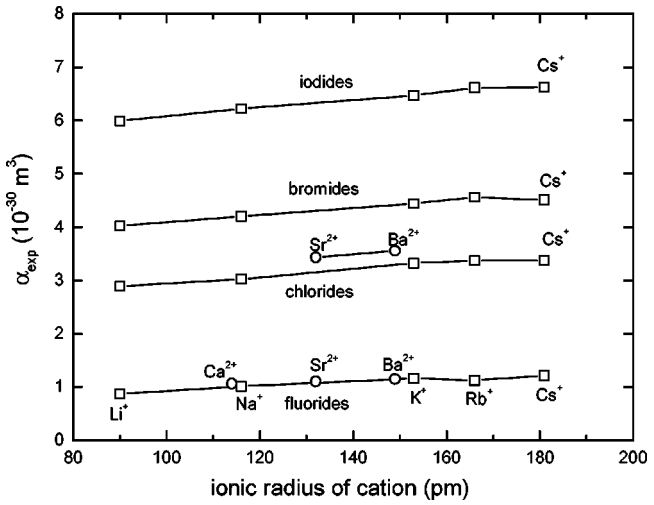

FIG. 8. Experimentally determined in-crystal anion polarizabilities α_{exp} in alkali- and alkaline-earth halides (data from Ref. 17) against the ionic radius of the cation.

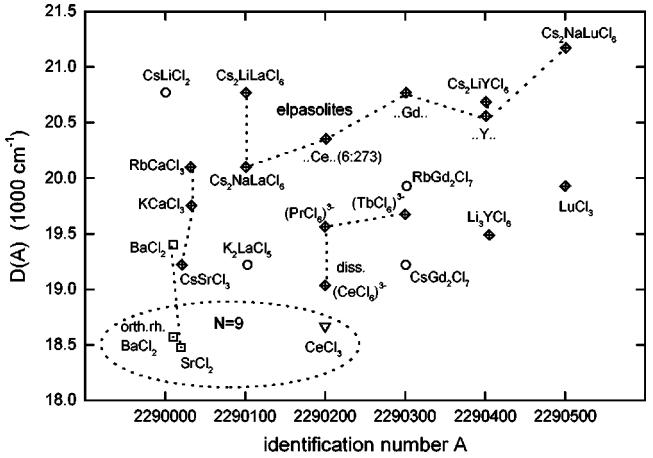

FIG. 9. Spectroscopic redshift in the chloride compounds. The errors are typically ±250 cm^{-1}.

D. Spectroscopic redshift

The results of the previous two sections on crystal field splitting and centroid shift will be combined here to discuss the redshift of the first fd transition of Ce^{3+} in a wider collection of chloride, bromide, and iodide compounds.

Figure 9 is a 10 000 times enlarged view of part of Fig. 1. On this scale the fifth digit (d_5) of the identification number (A) is of significance. It indicates the rare-earth site that is being occupied by the Ce^{3+} dopant. $d_5=1$ for La compounds and it increases with decreasing size of the cation until $d_5=5$ for Lu compounds. Increase of identification number tends to reflect increase of redshift (see Ref. 2). The smallest redshift values are found in the lower left corner of Fig. 9 and the largest ones in the top right corner.

The smallest redshift is observed for the compounds with ninefold coordination like $LaCl_3$ (not visible in Fig. 9), $CeCl_3$, $SrCl_2$ (C_{4v}), and orthorhombic $BaCl_2$. Crystal field splitting in these compounds is relatively small because of the large site size. Furthermore, the relatively large coordination number yields polyhedra that produce small crystal field splitting. This is particularly so for the tricapped trigonal prism coordination in $LaCl_3$. More details on $LaCl_3$ and $CeCl_3$, which have the same crystal structure, can be found in Ref. 13.

$RbGd_2Cl_7$ and $CsGd_2Cl_7$ have sevenfold coordination in the form of a monocapped trigonal prism (1ctp). It is to be expected that crystal field splitting in these compounds, like in K_2LaCl_5, will be relatively large resulting in larger redshift than the compounds with ninefold coordination.

All other compounds in Fig. 9 have sixfold coordination. Apart from NaCl and $CaCl_2$, the redshift values fall within a relatively narrow range from 19 000 to 21 000 cm^{-1}. Like observed for the fluorides (see Part I), the cubic chloride elpasolites Cs_2NaRCl_6 (R=La, Ce, Gd, Y, Lu) are the compounds with the largest redshift. The variations in centroid shift and crystal field splitting are quite subtle, see Fig. 2.

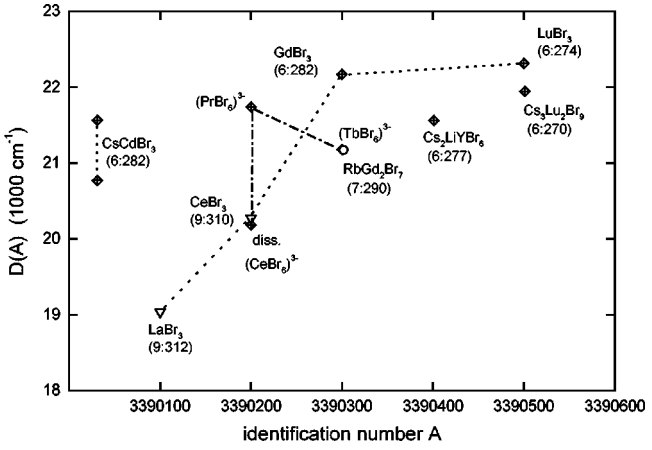

FIG. 10. Spectroscopic redshift in the bromide compounds. The errors are typically ± 250 cm^{-1}. Coordination number and R_{av} are occasionally given.

The combined effect results in an increase of redshift by about 1000 cm^{-1} in going from $Ca_2NaLaCl_6$ with the large La site to $Cs_2NaLuCl_6$ with the small Lu site.

Figure 10 is a 10 000 times expanded part of Fig. 1 and shows the redshift in the bromides as function of the identification number (A). All data fall within a relatively narrow range. $LaBr_3$ and $CeBr_3$ have the same crystal structure as $LaCl_3$ with ninefold (3ctp) coordination and like for the chlorides the smallest redshift is observed for these compounds. Apart from $RbGd_2Br_7$, the other compounds show sixfold (tap)- or (tp)-like coordination with redshift around 21 500 ± 800 cm^{-1}.

The only information available on Ce^{3+}-doped iodides stems from $Cs_3Gd_2I_9$ with $D(A)=23\,800$ cm^{-1}, see Fig. 1. Employing the ligand polarization model and the PCEM, this value will be used to predict the typical centroid shift and crystal field splitting in iodide compounds. It is assumed that the crystal structure is the same as that of $Cs_3Y_2I_9$ but with a 4 pm larger R^{3+} site size.[7] Coordination is then distorted octahedral ($\theta_{pr}\approx 50$) with C_{3v} site symmetry and $R_{av}-\frac{1}{2}\Delta R\approx 308$ pm. Extrapolating in Fig. 3 one expects $\epsilon_{cfs}\approx 13\,000\pm 2000$ cm^{-1}. Employing Eq. (1) with $r(A)=2.2\pm 0.2$ yields $\epsilon_c=19\,800\pm 1100$ cm^{-1}. Next employing Eq. (2) one obtains $\alpha_{sp}=19.6\pm 1.1\times 10^{-30}$ m^3. These predicted values are also shown in Table III and displayed in Fig. 7. It is assuring to see that the value for α_{sp} thus obtained is consistent with expectations based on Fig. 8. The difference in iodide and bromide polarizability in the alkali halides is larger than the difference between bromide and chloride polarizabilities. The same holds for the values of spectroscopic polarizability α_{sp} found in this work. It demonstrates once more the relationship between centroid shift of the 5d configuration and in-crystal anion polarizability.

E. Role of charge compensating defects

$CaCl_2:Ce^{3+}$ has the rutile structure and the Ca site is sixfold coordinated in the form of a distorted octahedron. Unexpectedly, a very small redshift related with a very small crystal field splitting of the 5d levels, see Fig. 2, is observed. The small splitting is not consistent with an octahedral coordination, see Fig. 3. It is known that under pressure, the rutile $CaCl_2$ transforms to the PbFCl type structure by means of a simple shift of cations (see p. 67 in Ref. 20). Then also coordination changes from octahedral to a tricapped trigonal prism. Possibly, assisted by a charge compensating defect, such coordination change also occurs locally around Ce^{3+} in $CaCl_2$. Like in $LaCl_3$ it will then yield relatively small crystal field splitting combined with relatively large Stokes shift of 5300 cm^{-1}.

NaCl has a redshift of 14 400 cm^{-1}, which is also very small for an octahedrally coordinated site. This together with the large Stokes shift of 6800 cm^{-1} also indicates that coordination is different from octahedral. Possibly charge compensation by means of replacement of a Na^+ by a Cl^- ion may accomplish such coordination changes.

In $CsCdBr_3$ (6:282) (octa:D_{3d}) two luminescing sites have been identified.[19] The site with the smallest redshift has been attributed by van Uitert[19] to Ce on a Cd site without charge compensation. The site with the largest redshift has been attributed to Ce–(Cd-vacancy)–Ce complexes. Note that a similar situation was encountered in $KMgF_3:Ce^{3+}$, see Part I. Also here charge compensation by means of K^+ vacancies yields larger redshift than the uncompensated site. It is interpreted as follows: a cation vacancy does not provide any attractive force on the anion charge cloud. Enhanced anion polarizability and centroid shift is then to be expected.

IV. SUMMARIZING REMARKS AND CONCLUSIONS

At the outset of the study on the 5d-level positions of the trivalent lanthanides in inorganic crystals, one of the first aims was to collect and critically analyze the data available. It provided a database with predictive potential. The next aim was to understand the relationship between the value for the redshift and the type of crystalline environment. For that purpose knowledge on the centroid shift and the crystal field splitting of the 5d levels was needed.

Crystal field splitting depends strongly on the shape and the size of the coordinating anion polyhedron. The point charge electrostatic model provides a convenient description for relating polyhedral shape and ϵ_{cfs}. In particular the angular part of the crystal field parameter B_0^4 calculated from the PCEM seems often to be a good indicator for the largeness of ϵ_{cfs}. The polyhedral size depends on the size of the substituted cation but more strongly on the size of the anions.

The ligand polarization model was employed to relate the centroid shift to one single parameter, the spectroscopic polarizability, which is independent on the coordination number and the metal to ligand distances in the structure. α_{sp} behaves as function of the type of cations and anions in the host crystal in the same manner as that of the actual in-crystal halide ion polarizability α_{exp} that can be derived from macroscopic properties. The spectroscopic polarizability α_{sp} increases according to

$$\text{anion vacancy} < F^- < Cl^- < Br^- < I^-. \qquad (6)$$

This ordering is the same as that of the well-known nephelauxetic series. By means of the values for α_{sp} now a quantitative interpretation is provided to this series.

The combined effect of centroid shift and crystal field splitting on the spectroscopic redshift in halogenide com-

pounds is summarized in Fig. 1. The vertical hatched blocks represent the (anticipated) range of centroid shift values. The range of contribution from the crystal field splitting to $D(A)$ is represented by the interval between the dashed lines. Its magnitude decreases by more than a factor of 2 in going from the fluorides to the iodides. The main reason for this is the increasingly larger ionic radius of the anions resulting in smaller crystal field splitting.

Within a halide group, the cations present in the crystal are important for variations in the redshift. Crystal field splitting for Ce^{3+} on large cation sites that require large coordination number is usually small. Small cations require small coordination number and crystal field splitting is large for Ce^{3+} on these sites. The cations are also important for the polarizability of the anions. The values for α_{sp} obtained by applying the ligand polarization model to the experimental data (see also Part I) appear to increase with the type of cation approximately as follows:

$$Mg^{2+}<Lu^{3+}<Th^{4+}<Y^{3+}<Li^{+}<La^{3+}<Ca^{2+}$$
$$<Na^{+}<Sr^{2+}<Ba^{2+}<K^{+}<Rb^{+}<Cs^{+}<\text{cation vacancy}, \quad (7)$$

where small high-valency cations are in the beginning of the series and large monovalency cations are at the end of the series. Note that the monovalent and divalent cations appear in sequence of increase of ionic radius, cf. Fig. 8.

It is not claimed in this work that the ligand polarization model is theoretically correct. Actually it is not. The assumptions made by Morrison to approximate the self-interaction will probably not hold for the extended $5d$ orbitals. Also the model as applied in this work ignores the contribution of the nephelauxetic effect and covalency to the centroid shift. Nevertheless, employing the model enables one to relate the centroid shift to one single parameter, i.e., the spectroscopic polarizability α_{sp}. The complexity of the crystal structure is then rigorously removed. The fact that α_{sp} varies more strongly than the actual anion polarizability α_{exp} may signal the contribution of covalency effects to the centroid shift.

Finally, there appears to be an intimate relationship between spectroscopic polarizability and the concept of optical basicity. Over the past 30 years many papers by Duffy *et al.* have appeared on the oxidic chemistry of glasses,[21] molten salts, and metallurgical slags.[22] The acid-base reactions in the molten state, i.e., the chemical basicity of the melt, are quite important in the glass-making and steel-making industry.[22] The basicity is directly related to the electron donating power of the anions, in this case oxygen. This donating power can be probed by measuring the spectroscopic redshift of the $^3P_1 \leftarrow {}^1S_0$ transition with Tl^+, Pb^{2+}, or Bi^{3+} dopants.[23] Based on the observed redshift, a so-called optical basicity scale has been developed that is used in oxidic chemistry.[24] The optical basicity Λ depends on the cations present in the melt. Small high-valency cations yield small Λ and large monovalent ones yield large Λ. Clearly the redshift of Tl^+, Pb^{2+} or Bi^{3+} in oxides and the centroid shift of Ce^{3+} in halides are caused by the same physical/chemical processes, and Λ and α_{sp} are intimately related parameters.

Binks and Duffy[25] also realized that optical basicity and in crystal oxygen polarizability are related. However, a model to relate both properties seems to be still lacking in the field of oxidic chemistry. The ligand polarization model applied in this work provides a direct link between (1) the centroid shift of the Ce^{3+} $5d$ configuration, (2) the optical basicity concept in oxidic chemistry, and (3) the anion polarizability derived from macroscopic properties. In the planned following papers of this series, where oxides and sulfide systems are the subject of study, these relationships will be more firmly established.

ACKNOWLEDGMENTS

The author wishes to thank J. Andriessen for critically reading this manuscript and for sharing his knowledge on the theory of crystal field interaction, Ce^{3+} energy level spectroscopy, and lattice relaxation studies in ionic crystals.

[1] P. Dorenbos, J. Lumin. **91**, 155 (2000).
[2] P. Dorenbos, J. Lumin. **91**, 155 (2000).
[3] Preceding paper, P. Dorenbos, Phys. Rev. B **62**, 15 640 (2000)
[4] Wei-Min Li and M. Leskelä, Mater. Lett. **28**, 491 (1996).
[5] O.T. Antonyak and N.S. Pidzyrailo, Opt. Spektrosk. **60**, 1198 (1986) [Opt. Spectrosc. **60**, 743 (1986)].
[6] O.T. Antonyak, A.S. Voloshinovskii, E.N. Mel'chakov, M.S. Mikhailik, M.S. Pidzyrailo, I.V. Stefanskii, and P.A. Rodnyi, Opt. Spektrosk. **84**, 950 (1998) [Opt. Spectrosc. **84**, 861 (1998)].
[7] G. Meyer, Prog. Solid State Chem. **14**, 141 (1982).
[8] C. Görller-Walrand and K. Binnemans, in *Handbook on the Physics and Chemistry of Rare Earths*, edited by K. A. Gschneidner, Jr. and L. Eyring (Elsevier Science B.V., Amsterdam, 1996), Vol. 23, Chap. 155.
[9] M.C. Favas and D.L. Kepert, Proc. Inorg. Chem. **28**, 309 (1981).
[10] A. Zalkin and D.H. Templeton, Acta Crystallogr., Sect. B: Struct. Sci. **41**, 91 (1985).
[11] J.S. Griffith, *The Theory of Transition-metal Ions* (Cambridge University Press, London, 1961).
[12] P. Dorenbos, J. Andriessen, M. Marsman and C.W.E. van Eijk, Radiat. Eff. Defects Solids (to be published).
[13] J. Andriessen, O.T. Antonyak, P. Dorenbos, P.A. Rodnyi, G.B. Stryganyuk, C.W.E. van Eijk, and A.S. Voloshinovskii, Opt. Commun. **178**, 355 (2000).
[14] M. Marsman, H. Andriessen, and C.W.E. van Eijk, Phys. Rev. B **61**, 16 477 (2000).
[15] M.F. Reid, L. van Pieterson, R.T. Wegh, and A. Meijerink, Phys. Rev. B (unpublished).
[16] W.J. Manthey, Phys. Rev. B **8**, 4086 (1973).
[17] E.W. Pearson, M.D. Jackson, and R.C. Gordon, J. Phys. Chem. **99**, 119 (1984).
[18] R.D. Shannon, Acta Crystallogr., Sect. A: Cryst. Phys., Diffr., Theor. Gen. Crystallogr. **32**, 751 (1976).
[19] L.G. van Uitert, J. Lumin. **29**, 1 (1984).
[20] B.G. Hyde and S. Andersson, *Inorganic Crystal Structures* (Wiley, New York, 1989).
[21] J.A. Duffy and M.D. Ingram, J. Non-Cryst. Solids **21**, 373 (1976).
[22] J.A. Duffy and M.D. Ingram, J. Chem. Soc., Faraday Trans. 1 **74**, 1410 (1978).
[23] J.A. Duffy and M.D. Ingram, J. Am. Chem. Soc. **93**, 6448 (1971).

[24] J.A. Duffy and M.D. Ingram, J. Inorg. Nucl. Chem. **37**, 1203 (1975).
[25] J.H. Binks and J.A. Duffy, J. Chem. Soc., Faraday Trans. 2 **81**, 473 (1985).
[26] J.C. van't Spijker, P. Dorenbos, C.W.E. van Eijk, K. Krämer, and H.U. Güdel, J. Lumin. **85**, 1 (1999).
[27] R_{av} obtained from the cell volume reported by M.C. Marco De Lucas, F. Rodriquez, C. Prieto, M. Verdaguer, and H.U. Güdel, J. Phys. Chem. Solids **7**, 995 (1995).
[28] J.C. van't Spijker, P. Dorenbos, C.W.E. van Eijk, M.S. Wickleder, H.U. Güdel, and P.A. Rodnyi, J. Lumin. **72-74**, 786 (1997).
[29] A. Sidorenko, Interfaculty Reactor Institute Report No. ST-ISO-2000-007, 2000 (unpublished).
[30] R.W. Schwartz and P.N. Schatz, Phys. Rev. B **8**, 3229 (1973).
[31] C.M. Combes, P. Dorenbos, C.W.E. van Eijk, K.W. Krämer, and H.U. Güdel, J. Lumin. **82**, 299 (1999).
[32] R_{av} was estimated from D.H. Templeton and G.F. Carter, J. Phys. Chem. **58**, 940 (1954) by comparing the cell volume with that of YCl_3.
[33] O. Guillot-Noël, J.T.M. de Haas, P. Dorenbos, C.W.E. van Eijk, K. Krämer, and H.U. Güdel, J. Lumin. **85**, 21 (1999).
[34] Estimated from $GdBr_3$ [H.H. Thomas, Acta Crystallogr., Sect. B: Struct. Crystallogr. Cryst. Chem. **29**, 1740 (1973)].